

First two energy levels in ^{15}F

W. A. Peters,^{1,2} T. Baumann,¹ D. Bazin,¹ B. A. Brown,^{1,2} R. R. C. Clement,¹ N. Frank,^{1,2} P. Heckman,^{1,2} B. A. Luther,^{1,*} F. Nunes,^{1,2} J. Seitz,^{1,2} A. Stoltz,¹ M. Thoennessen,^{1,2} and E. Tryggestad^{1,†}

¹National Superconducting Cyclotron Laboratory, Michigan State University, East Lansing, MI, 48824

²Department of Physics and Astronomy, Michigan State University, East Lansing, MI 48824

(Dated: Draft: June 9, 2003)

The ground state and first excited state of ^{15}F were measured by the method of elastic resonance scattering in inverse kinematics. A secondary beam of 115 MeV/nucleon ^{14}O was slowed down to 8 MeV/nucleon and energy bunched before stopping in a C_2H_4 target. The ^{15}F excitation energy spectrum was extracted from elastically scattered protons at 0° . The $1/2^+$ ground state resonance of ^{15}F was determined to be unbound with respect to single proton emission by 1.51 ± 0.11 MeV, corresponding to a mass excess of 16.81 ± 0.11 MeV. The $5/2^+$ first excited state resonance is unbound by 2.853 ± 0.045 MeV leading to an excitation energy of 1.34 ± 0.15 MeV. A comparison with systematics of single nucleon separation energies and theoretical models suggests that ^{11}N should be unbound by about 1.5 ± 0.15 MeV.

PACS numbers: 27.20.+n; 25.40.Cm; 25.60.Bx; 21.10.Dr

I. INTRODUCTION

The emergence and disappearance of (sub-)shells is a crucial observable in the understanding of nuclear structure as one approaches the driplines. The breakdown of the $N = 8$ shell closure near the neutron dripline has been established for ^{12}Be [1] and ^{11}Li [2]. The ground states of these nuclei exhibit significant $(1s, 0d)^2$ contributions in addition to the normal $(0p)^8$ configuration. The existence of a shell closure can also be deduced from the presence of a drop in the nucleon separation energy for nuclei with constant isospin [3, 4]. Figure 1(a) displays the relevant neutron separation energies (S_n) for the neutron-rich nuclei near the $N = 8$ shell. For nuclei with an isospin of $T_z = 1/2$, the one-neutron separation energy drops between ^{13}C and ^{17}O , while it increases monotonically with neutron number for the $T_z = 3/2$ isospin nuclei. The increase in separation energy from ^{11}Be to ^{15}C indicates the disappearance of the $N = 8$ shell closure [4].

Similar observations should also reveal any changes of the shell structure of the mirror nuclei at the proton dripline [3]. The situation for the $Z = 8$ shell differs from the $N = 8$ shell because the relevant nuclei for $T_z = -3/2$, ^{11}N and ^{15}F , are already unbound. The first experiment on ^{11}N detected the $p_{1/2}$ first excited state [5]. The existence and location of the $s_{1/2}$ ground state was only inferred from the mirror nucleus ^{11}Be , leading to an adopted value for the mass excess of 24.89 ± 0.2 MeV corresponding to a one-proton decay energy (inversion of the separation energy) of 1.90 ± 0.2 MeV [6]. Since then, several different experiments have ascertained the energy of the unbound $s_{1/2}$ ground state [7–11]. These

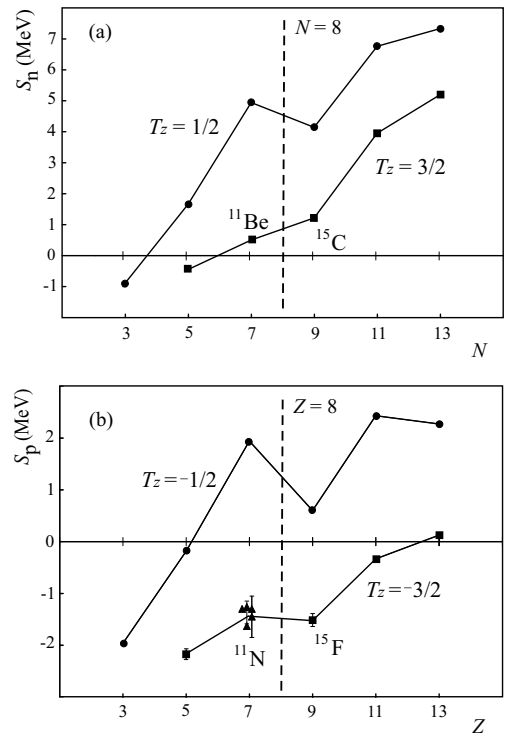


FIG. 1: Single nucleon separation energies. (a) S_n for neutron-rich $T_z = 1/2$ (circles) and $T_z = 3/2$ (squares) nuclei. The $N = 8$ shell closure has clearly disappeared for the $T_z = 3/2$ line. (b) S_p for proton-rich $T_z = -1/2$ (circles) and $T_z = -3/2$ (squares) nuclei. Triangles represent the most recent values for ^{11}N as reported in Refs. [7–11].

recent experiments on ^{11}N yielded significantly reduced proton decay energies making ^{11}N less unbound than ^{15}F . This leads to a drop in the one-proton separation energy at $Z = 8$, in direct contrast to the mirror nuclei. In Figure 1(b), the one-proton separation energies (S_p) for $T_z = -3/2$ nuclei are plotted (triangles represent the five recent values for the ^{11}N proton decay energy). The

*On leave from: Department of Physics, Concordia College, Moorhead, MN 56562

†Present address: Institut de Physique Nucléaire, IN2P3-CNRS, 91406 Orsay Cedex, France

slight drop in separation energy might imply the continued presence of the $Z = 8$ shell. However, the level inversion from a $p_{1/2}$ to a $s_{1/2}$ ground state in ^{11}N shows that the shell closure has indeed disappeared. This discrepancy could be resolved if ^{11}N had a larger one-proton decay energy or that of ^{15}F was smaller than previously reported.

The first experiments on ^{15}F observed the $s_{1/2}$ ground state in addition to the $d_{5/2}$ first excited state [12, 13]. The values reported in Refs. [12] and [13] lead to an adopted value for the one-proton decay energy of 1.47 ± 0.13 MeV [14]. Up to now, the ground state of ^{15}F has not been revisited. The unresolved question about the relative position of the ^{11}N and ^{15}F ground states and the marginal statistics in the measurement of the latter warranted a new investigation of ^{15}F . In the present study, we utilized a secondary beam of ^{14}O to populate the first two energy levels in ^{15}F with the method of elastic resonance scattering in inverse kinematics.

II. EXPERIMENTAL PROCEDURE

The experiment was performed at the Coupled Cyclotron Facility (CCF) of the National Superconducting Cyclotron Laboratory (NSCL) at Michigan State University. ^{16}O nuclei accelerated by the K500×K1200 coupled cyclotrons to 155 MeV/nucleon bombarded a 1900-mg/cm²-thick beryllium production target. The secondary ^{14}O beam was selected by the A1900 fragment separator [15]. An achromatic 971 mg/cm² acrylic wedge at the mid-focal plane was used to achieve better isotopic separation producing an 85% pure ^{14}O beam at 115 MeV/nucleon with a 15% contamination of ^{13}N . For elastic resonance scattering in inverse kinematics, the projectiles were stopped in a polyethylene reaction target. The secondary beam had to be slowed down significantly to energies below 10 MeV/nucleon which was achieved by a 5500-μm-thick aluminum energy degrader located at the object of the analysis beam line of the S800 spectrometer [16].

A mono-energetic wedge made from a curved aluminum foil with an effective thickness of 93.6 μm was placed at the dispersive plane of the analysis beam line to reduce the large energy spread caused by the degradation of the beam. Faster particles pass through more matter than slower particles, causing the energy spread to narrow to a fraction of its original size. This method is also referred to as energy bunching [17]. A nearly mono-energetic beam of 10.71 MeV/nucleon ^{14}O with a spread of only 0.084 MeV/nucleon or 0.8%, a reduction of a factor of approximately four compared to the beam in front of the wedge, was achieved. Figure 2 shows this method for a more intense high-energy secondary ^{15}O beam.

A 75 μm silicon detector was inserted in front of the target to identify and discriminate against beam contaminants. This further reduced the energy of the ^{14}O entering the polyethylene target to 7.98 MeV/nucleon with

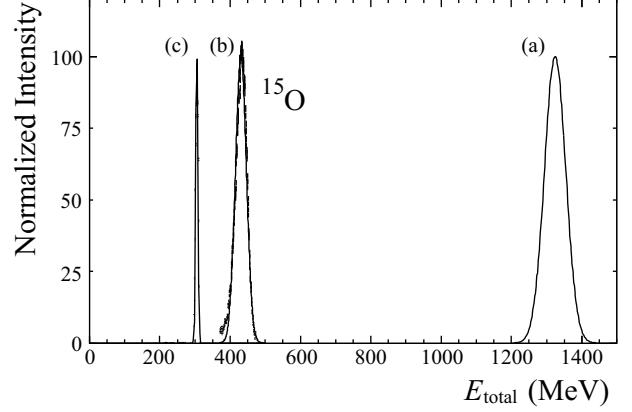


FIG. 2: Energy bunching of high-energy secondary ^{15}O test beam using a 312 μm mono-energetic Al wedge. (a) Gaussian distribution representing the 86 MeV/nucleon beam before a 6000 μm Al degrader. (b) Measured distribution of 28.8 MeV/nucleon beam with a spread of 3.4% before the mono-energetic wedge. (c) Final measured distribution of ^{15}O beam with 20.3 MeV/nucleon and a spread of only 1.0%.

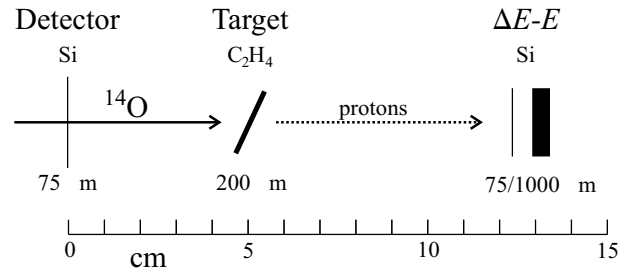


FIG. 3: Experimental setup. ^{14}O nuclei pass through a thin silicon detector and get stopped inside a polyethylene (C_2H_4) target with an effective thickness of 200 μm. Protons are scattered and then detected at 0° by a silicon ΔE - E telescope.

a spread of 0.12 MeV/nucleon or 1.5%. The secondary beam intensity at the reaction target averaged 2×10^3 particles per second. Transmission efficiency for this setting was not measured.

Figure 3 shows the experimental setup. The ^{14}O projectiles were stopped in a 181.3 μm polyethylene (C_2H_4 , $\rho = 0.933 \text{ g/cm}^3$) target rotated 25° for an effective thickness of 200 μm. Elastic scattering occurs at decreasing energies as the projectile slows down inside the target. The elastically scattered protons had sufficient energy to leave the target and were detected at 0° (180° in the center of mass) in a ΔE - E telescope consisting of 75.3 μm and 1000 μm silicon detectors. The bore diameter of the preceding quadrupole magnet limited the range of possible angles onto the target to 7°.

III. DATA ANALYSIS

The detectors were calibrated using α sources and protons scattered off the ^{13}N contaminant in the beam re-

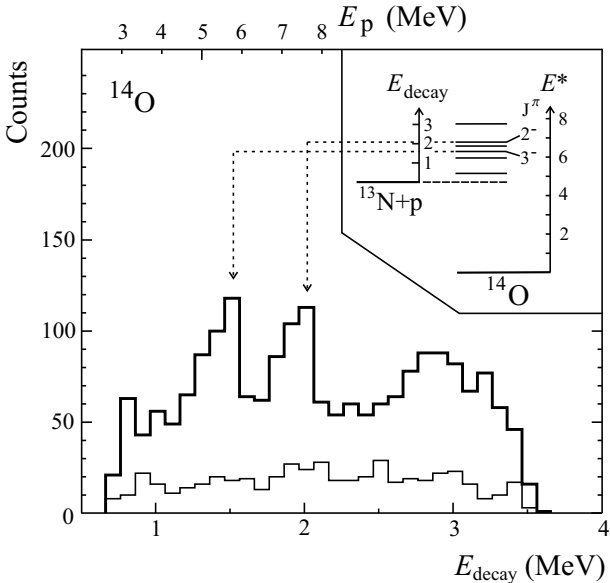


FIG. 4: Excitation spectrum of ^{14}O . The bold line corresponds to the experimental data using the polyethylene target while the thin line represents the background data with the carbon target. Proton energy measured in the lab is labeled on the top x axis and the calibrated energy above proton decay (center-of-mass) on the bottom. The inset shows the ^{14}O level scheme with the decay energy scale next to it.

vealing known excitation levels in ^{14}O . Incoming ^{14}O and ^{13}N projectiles were separated by time-of-flight measured between the silicon detector in front of the target and the cyclotron rf. A 12 ns difference between the two nuclei was sufficient to gate on either $(^{14}\text{O} + \text{p})$ or $(^{13}\text{N} + \text{p})$ events. Figure 4 shows the proton spectrum in coincidence with incoming ^{13}N nuclei and the corresponding ^{14}O level scheme. Two odd-parity states at excitation energies of 6.27 MeV (3^-) and 6.79 MeV (2^-) are clearly visible. In addition, the broader peak at higher energies corresponds most likely to the 2^+ state at 7.77 MeV. Odd-parity states are more strongly populated by proton scattering since an $l = 2$ proton can easily couple to the ground state of ^{13}N forming either the 2^- or 3^- state [18]. Other energy levels within the region of interest do not have simple single-particle configurations and are therefore suppressed.

Measured proton energies had to be corrected for the energy-loss inside the target after the scattering reaction. Scattering at higher energies occurs further from the back of the target, while scattering at lower energies occurs closer to the back as the projectile comes to rest. Thus, higher energy protons pass through more material compared to lower energy protons as they exit the target. For example, a 3 MeV proton (in center-of-mass frame) travels through 52 μm to exit the target, losing 22 keV of energy. By comparison, a 2 MeV proton exits through 31 μm of the target material and loses 18 keV. The corrected proton energy measured in the laboratory can then be directly converted to decay energy (energy

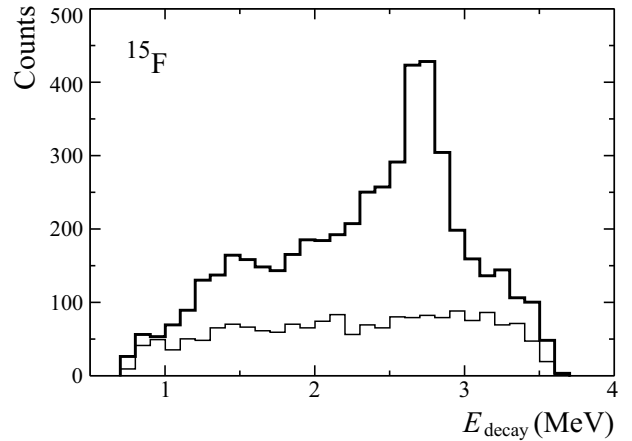


FIG. 5: Excitation spectrum of ^{15}F . The bold line represents the experimental data taken with the polyethylene target while the thin line corresponds to the data from the carbon target measurement.

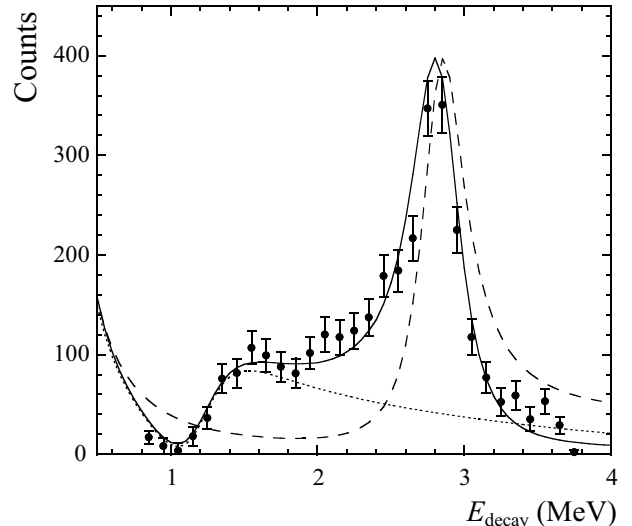


FIG. 6: Fitted excitation spectrum of ^{15}F . The solid line corresponds to the cross section curve for both resonances together. The dotted and dashed lines characterize the single cross section curves for the $s_{1/2}$ and $d_{5/2}$ states, respectively. Our data points are shown as solid circles with statistical error bars.

above the proton separation energy of ^{15}F):

$$E_{\text{decay}} = \frac{M(^{14}\text{O}) + m_{\text{p}}}{4 M(^{14}\text{O})} E_{\text{p}}$$

The low-energy cut-off of the total energy plot is determined by the protons that stop in the ΔE detector. For these events no particle identification was possible. At higher energies, the spectrum is limited by protons that do not stop in the E detector.

In addition to the polyethylene target, data were also taken with a pure carbon target in order to subtract background events from protons that scattered off the carbon

TABLE I: Parameters for the potential model fit.

$V_{WS}(d_{5/2})$	-49.06 MeV
$V_{WS}(s_{1/2})$	-48.01 MeV
V_{LS}	4.50 MeV
$r_0(WS)$	1.25 fm
$r_0(LS)$	1.25 fm
$r_0(\text{Coulomb})$	1.25 fm
$d(WS)$	0.75 fm
$d(LS)$	0.75 fm

content in the polyethylene (Figures 4 & 5). Figure 6 shows the final ^{15}F energy spectrum (solid circles) after subtraction of the carbon contribution. The spectrum looks qualitatively similar to the data taken for ^{11}N with the same method [7, 8]. At low energies the tail of the Coulomb scattering is visible. A broad peak emerges at approximately 1.5 MeV and a sharp peak is located at 2.8 MeV.

The relative energy uncertainty is estimated to be 50 keV, which is dominated by the angular and energy straggling (calculated by LISE [19], energy-loss according to Ziegler [20]) accounting for roughly 1.5% and 0.3%, respectively, of the scattered proton energy. The 1.5% uncertainty also includes the effect due to the angular acceptance after the target of 8.5° . This angular acceptance had no effect on the position of the cross section maxima.

IV. RESULTS AND DISCUSSION

The data were compared with results from potential model calculations using the program VLADCS [21] that incorporates a standard Woods-Saxon potential with Coulomb and spin-orbit terms added. It provides the relative cross sections for single-particle resonances as a function of proton scattering energy, taking interference effects into account. This simulated cross section distribution is directly comparable with our measured energy spectrum.

The solid line in Figure 6 corresponds to a fit using the parameters listed in Table I. The result of the simulation was folded with the experimental energy spread using a Gaussian distribution with 50 keV width. Including the experimental energy spread had only a negligible effect on the overall shape of the spectrum. Individual contributions from the $s_{1/2}$ and $d_{5/2}$ states are shown as dotted and dashed lines, respectively. The very broad shape of the first resonance confirms the $s_{1/2}$ nature of the ground state. Interference between the two positive parity states accounts for the relative energy shift especially visible for the $d_{5/2}$ state.

The maximum of the cross section is at a decay energy of 1.51 ± 0.11 MeV for the ground state and at 2.853 ± 0.045 MeV for the first excited state. The latter corresponds to an excitation energy of 1.34 ± 0.15 MeV.

TABLE II: ^{15}F decay energies determined by the maximum of the scattering cross section (σ_{\max}), using the S -matrix pole, the 90° crossing of the phase shift ($\delta = 90^\circ$), and from the maximum of the partial wave-function at a radius of 1 fm ($\Psi_{\max} @ 1 \text{ fm}$). Values are given in MeV.

	σ_{\max}	S -matrix pole	$\delta = 90^\circ$	$\Psi_{\max} @ 1 \text{ fm}$
$s_{1/2}$	1.51	1.48	1.47	1.29
$d_{5/2}$	2.853	2.87	2.87	2.85

These values are in agreement with the previous measurements of ^{15}F [12, 13] and the adopted value for the mass of ^{15}F [14]. The uncertainty of the maximum cross section value of the ground state is dominated by the broad nature of the state and statistics, while for the first excited state it is dominated by the uncertainty of the energy calibration. The width (FWHM) of the first excited state is 340 keV. As pointed out by Benenson *et al.* [13], the width of the ground state is hard to quantify due to the missing angular momentum barrier of the $s_{1/2}$ state which results in a large tail towards higher energies. Nevertheless, we determined the full width at half maximum for the $s_{1/2}$ resonance to be 1.2 MeV.

While nucleon separation energies for bound nuclei and states are well defined, there are different theoretical methods to define the separation energy of unbound states or resonances. Table II displays the various values of the decay energies of the first two energy levels in ^{15}F that we deduced from our experimental data using VLADCS. The first column lists decay energies determined by the maxima of the cross sections. The values extracted using the S -matrix pole and the 90° crossing of the phase shift (second and third column) agree with the maximum of the cross section values within the uncertainties. Only the method of extracting the resonant energy from the maximum of the partial wave-function at a radius of 1 fm (last column) yields a significantly smaller value for the $s_{1/2}$ resonance energy.

Since our current measurement confirms the position of the ^{15}F ground state and first excited state, the perceived contradiction between the vanishing of the $Z = 8$ shell closure and the apparent presence of a drop in the proton separation energy for the $T_z = -3/2$ isospin nuclei shown in Figure 1(b) must be resolved differently. Before discussing the large variance of experimental results for the ground state of ^{11}N , we investigate a few theoretical predictions for the masses of ^{11}N and ^{15}F .

The isobaric mass multiplet equation cannot be used for a comparison of ^{11}N and ^{15}F , because the $A = 15$, $T = 3/2$ quartet is incomplete [22]. The $1/2^+$ analog state in ^{15}O has not been identified.

Several theoretical models with parameters fitted to the mirror nuclei ^{11}Be and ^{15}C predict similar one-proton separation energies for the ground states of ^{11}N and ^{15}F . Grevy, Sorlin and Vinh Mau [23] calculate a decay energy of 1.2 MeV for both nuclei using a potential model with an extra surface term. Computations we completed using

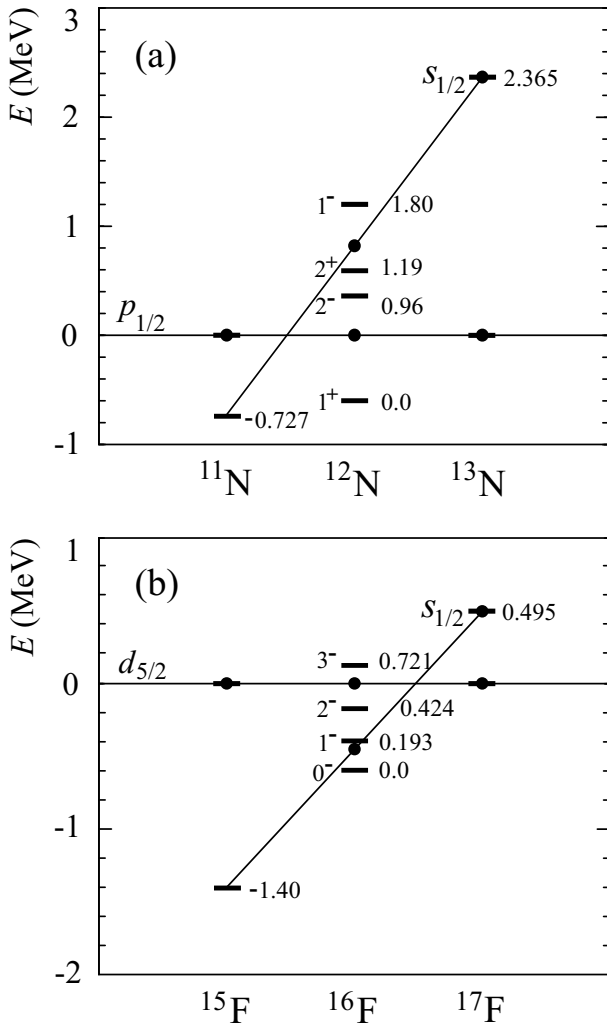


FIG. 7: Talmi extrapolation for (a) $Z = 7$, and for (b) $Z = 9$. A linear fit to the $s_{1/2}$ state relative to the (a) $p_{1/2}$ and (b) $d_{5/2}$ levels illustrates that as the neutron number decreases so does the difference in energy between these states. For the even-mass nuclei (a) ^{12}N , and (b) ^{16}F , the pairs of relevant $s_{1/2}$, $p_{1/2}$ and $d_{5/2}$ analog levels weighted by $(2j+1)$ was used to calculate the average position for the linear fit.

a single-particle model yield 1.43 MeV and 1.38 MeV for the ground states of ^{11}N and ^{15}F , respectively. While these calculations yield slightly lower energies than our measured value for the ^{15}F ground state, both predict that ^{11}N and ^{15}F should have similar proton separation energies.

Further support for the decay energies of the ^{11}N and ^{15}F ground states being nearly equal can be deduced from a simple extrapolation first used by Talmi and Unna for the mirror nuclei ^{11}Be and ^{15}C [24]. They implemented this extrapolation to explain the $p_{1/2}$ - $s_{1/2}$ and $d_{5/2}$ - $s_{1/2}$ level inversions in these nuclei. This method postulates a linear decrease in the $s_{1/2}$ energy level with respect to $p_{1/2}$ or $d_{5/2}$ as the nucleon number decreases. The reasons for these inversions are certainly much more com-

plicated than expressed in this extrapolation [1], nevertheless it predicted the correct decay energies to within 110 keV.

This technique can be applied to the mirror nuclei ^{11}N and ^{15}F as shown in Figure 7. The level positions for ^{12}N and ^{16}F were determined from the average of the two analog states weighted by $(2j+1)$. After the inversion energy to the $s_{1/2}$ levels are known, a simple subtraction from the more accurate measurements of the first excited states leads to the energy of the related ground state. A linear extrapolation from ^{13}N and ^{12}N to ^{11}N predicts the $s_{1/2}$ state to be 727 keV below the $p_{1/2}$ state, for a decay energy of 1.37 MeV. Similarly, for ^{15}F the $s_{1/2}$ state is estimated to be 1.40 MeV below the $d_{5/2}$ excited state, leading to a similar decay energy of 1.45 MeV. It should be noted that the level inversion in the fluorine isotopes appears first in proton-unbound ^{16}F , as the 0^- and 1^- ($s_{1/2}$) states are below the 2^- and 3^- ($d_{5/2}$) states.

The theoretical predictions thus indicate that the vanishing of the $Z = 8$ shell closure does not imply that the separation energy of the isotope just below the shell is less than the isotope just above the shell for constant isospin, contrary to the case for the $N = 8$ shell closure (see Figure 1). The calculations predict that the separation energies are nearly equal. With the present confirmation of the mass of ^{15}F these calculations can then be used to deduce the ground state of ^{11}N to be unbound by 1.5 ± 0.15 MeV.

As we have pointed out, it is not always trivial to compare experimental values of nucleon separation energies of unbound states since various methods can be used to extract these values. This is also the case for the reported experimental decay energies of ^{11}N plotted in Figure 1(b). The most recent values for the ^{11}N decay energy, 1.47 ± 0.4 MeV [9], 1.63 ± 0.05 MeV [10], and 1.31 ± 0.05 MeV [11], all refer to the maximum of the resonant scattering cross section, analogous to the first column in Table II. Results reported by Axelson *et al.* (1.30 ± 0.04 MeV [7]) and Markenroth *et al.* ($1.27^{+0.18}_{-0.05}$ MeV [8]), are deduced using the maximum of the partial wave-function at 1 fm, yielding a lower value for the decay energy as compared to the maximum of the scattering cross section (as observed for ^{15}F in Table II). A closer look at the data of Refs. [7] and [8] reveals that the cross section maximum for the $s_{1/2}$ resonance is indeed at a higher energy than the quoted values of 1.27 MeV and 1.30 MeV, namely at roughly 1.40 MeV. Considering this, all of the previously reported values except for the most recent measurement by Guimarães *et al.* [11] agree with the presently deduced value for the ground state energy of ^{11}N .

V. SUMMARY AND CONCLUSIONS

The mass and first excited state of ^{15}F was measured using the method of elastic resonance scattering in inverse kinematics. ^{15}F is unbound with respect to one-

proton decay by 1.51 ± 0.11 MeV corresponding to a mass excess of 16.81 ± 0.11 MeV. The first excited state was measured at an excitation energy of 1.34 ± 0.15 MeV, unbound by 2.853 ± 0.045 MeV. These values agree with the two original measurements of ^{15}F [12, 13]. Considering the systematics of single nucleon separation energies for constant isospin as well as various theoretical calculations, both ^{11}N and ^{15}F should have nearly equal proton separation energies despite the level inversion in ^{11}N establishing that the $Z = 8$ shell vanishes. By confirming the mass of ^{15}F it is suggested that ^{11}N is unbound by

1.5 ± 0.15 MeV.

Acknowledgements

This work has been supported by the National Science Foundation grants PHY01-10253 and PHY00-70911. We would like to thank I. J. Thompson for valuable discussions and G. Rogachev and N. Vinh Mau for making the potential model codes available.

-
- [1] A. Navin *et al.*, Phys. Rev. Lett. **85**, 266 (2000).
 - [2] H. Simon *et al.*, Phys. Rev. Lett. **83**, 496 (1999).
 - [3] A. Bohr and B. R. Mottelson, *Nuclear Structure*. Vol. 1 p. 192, W. A. Benjamin, New York, Amsterdam, (1969).
 - [4] A. Ozawa, T. Kobayashi, T. Suzuki, K. Yoshida, and I. Tanihata, Phys. Rev. Lett. **84**, 5493 (2000).
 - [5] W. Benenson, E. Kashy, D. H. Kong-A-Siou, and H. Nann, Phys. Rev. C **9**, 2130 (1974).
 - [6] F. Ajzenberg-Selove, Nucl. Phys. **A506**, 1 (1990).
 - [7] L. Axelsson *et al.*, Phys. Rev. C **54**, R1511 (1996).
 - [8] K. Markenroth *et al.*, Phys. Rev. C **62**, 034308 (1998).
 - [9] A. Azhari *et al.*, Phys. Rev. C **57**, 628 (1998).
 - [10] J. M. Oliviera *et al.*, Phys. Rev. Lett. **84**, 4056 (2000).
 - [11] V. Guimarães *et al.*, Phys. Rev. C **67**, 064601 (2003).
 - [12] G. J. Kekelis, M. S. Zisman, D. K. Scott, R. Jahn, D. J. Vieira, J. Cerny, and F. Ajzenberg-Selove, Phys. Rev. C **17**, 1929 (1978).
 - [13] W. Benenson, E. Kashy, A. G. Ledebuhr, R. C. Pardo, R. G. H. Robertson, and L. W. Robinson, Phys. Rev. C **17**, 1939 (1978).
 - [14] F. Ajzenberg-Selove, Nucl. Phys. **A523**, 1 (1991).
 - [15] D. J. Morrissey, B. M. Sherrill, M. Steiner, A. Stolz, I. Wiedenhöfer, Nucl. Instr. and Meth. B **204**, 90 (2003).
 - [16] D. Bazin, J. A. Caggiano, B. M. Sherrill, J. Yurkon, A. Zeller, Nucl. Instr. and Meth. B **204**, 629 (2003).
 - [17] H. Weick *et al.*, Nucl. Instr. and Meth. B **164-165**, 168 (2000).
 - [18] G. C. Ball and J. Cerny, Phys. Rev. **177**, 1466 (1969).
 - [19] D. Bazin *et al.*, Nucl. Instr. and Meth. A **482**, 307 (2002).
 - [20] J. F. Ziegler, J. P. Biersack, U. Littmark, *The Stopping and Range of Ions in Solids*. Vol. 1, Pergamon Press, New York, (1985).
 - [21] G. Rogachev, private communication.
 - [22] G. W. Phillips *et al.*, Phys. Rev. C **5**, 297 (1972).
 - [23] S. Grevy, O. Sorlin, and N. Vinh Mau, Phys. Rev. C **56**, 2885 (1997).
 - [24] I. Talmi and I. Unna, Phys. Rev. Lett. **4**, 469 (1960).